Characterisation of overloads in fatigue by 2D strain mapping at the surface and in the bulk

P. Lopez-Crespo[1]♣, M. Mostafavi[2], A. Steuwer[3],
J. F. Kelleher[4], T. Buslaps[5], P. J. Withers[6]

[1]*Department of Civil and Materials Engineering, University of Malaga, C/ Doctor Ortiz Ramos, s/n, 29071, Malaga, Spain*
[2]*Department of Mechanical Engineering, University of Bristol, Queen's Building, University Walk, Bristol BS8 1TR UK*
[3]*NMMU, Gardham Avenue, Port Elizabeth 6031, South Africa*
[4]*ISIS, Rutherford Appleton Laboratory, Didcot, Oxfordshire OX11 0QX, UK*
[5]*ESRF, 6 rue J Horowitz, 38000 Grenoble, France*
[6]*School of Materials, University of Manchester, Manchester M13 9PL, UK*

ABSTRACT.

Two complementary experimental techniques have been used to study the evolution of crack-tip strain fields in a thin (plane stress dominated) compact tension sample following a single overload (OL) event. The total strain has been characterised at the surface by Digital Image Correlation (DIC), while the elastic strain field in the bulk (interior) behaviour has been characterised by means of synchrotron X-ray diffraction (XRD). Surface and bulk information allowed us to visualise the evolution of the strain fields before the OL event, during the OL event, just after it and at various stages after it. Unlike previous work, complete 2D maps of elastic strains around the crack-tip were acquired at 60μm spatial resolution by XRD. The strain data were used to estimate the effective crack driving force at the surface and at the mid plane. The DIC shows less crack opening displacement after overload and the XRD a lower crack-tip peak stress after OL until the crack has grown past the compressive crack-tip residual stress after which the behaviour returned to that for the baseline fatigue response. While the compressive residual stress introduced by the OL offsets the crack-tip stress field as it grows through the overload plastic zone, the changes in crack-tip stress over each cycle are the same before and at all stages after OL.

KEYWORDS

Linear elastic fracture mechanics, crack closure, plastic strain, bainitic steel, effective stress intensity factor.

♣ Corresponding author: plopezcrespo@uma.es

1. INTRODUCTION

Engineering components such as aircraft structures, pressure vessels or rotating machinery are only rarely subjected to constant amplitude fatigue, often experiencing overloads. It is well known that such overload events can drastically decrease the propagation rate of fatigue cracks, or even result in crack arrest. Mechanisms such as crack-tip blunting [1], crack branching [2], crack-tip strain hardening [3] and crack closure [4] have been suggested to explain the retardation in crack growth rate following overload. Nevertheless the underlying mechanisms controlling such behaviour are not fully understood [5]. Closure of the crack-faces either near to, or distant from, the crack-tip means that the crack-tip does not experience the full crack-opening fatigue cycle. Such effects have been held to be responsible for the immediate acceleration and then subsequent retardation of the crack growth rate observed following an overload during fatigue cycling.

Diffraction peak shifts are predominantly sensitive to the elastic strain and a number of studies have mapped the strain ahead of, and behind, the crack-tip using neutron [6, 7] or synchrotron x-ray [8-10] beams. The problem with line-scans along the crack plane is that there is a danger that the location of the peak stress may be missed. Steuwer et al. [11] were the first to map the stresses in thick (plane strain) samples in 2D at high (25μm) resolution with X-ray diffraction (XRD), but in their case the plastic zone was small and the crack-tip stress fields dominated largely by elastic behaviour.

In this paper, we employ Digital Image Correlation (DIC), a non-contact full-field measurement technique, to measure the total (elastic plus plastic) strain on the surface of the specimen. The accuracy of DIC to measure elastic strain is debateable, but its capability to measure total strain (considering that plastic strains are normally few times bigger than elastic strains) is unrivalled [12]. DIC has found increasing application for the study of crack-tip strain fields [13] and it has been possible to extract fracture mechanics information such as closure stresses [14, 15], plastic zone sizes [16], crack-tip opening displacements (COD) [17] and effective stress intensity factors at the crack-tip, K_{eff} [12, 16, 18-20].

The combination of the two techniques provides both elastic (from XRD) and total (DIC) strains if the measurements are carried out at the same locations. Consequently, we adopted a thin (i.e. plane stress dominated) specimen compact tension geometry so that the variation of the strain field on the surface, where DIC measures the total strain, and the elastic strain averaged through thickness as measured by XRD, is minimised.

Lopez-Crespo et al. have already combined these complementary methods to examine the strain fields local to a crack-tip in a plane stress (thin) stainless steel compact tension sample prior and subsequent to an overload event [21]. Even under plane stress where the surface and bulk states might be expected to be the same, important differences were observed between DIC and XRD. Surface DIC measurements suggested that under fatigue cycling the cracks faces appear to be in contact for around 50% of the cycle supporting a traditional plasticity-induced closure interpretation. Indeed they observed a drastic change in the COD versus load curve in the closure response for baseline fatigue prior to overload, an absence of closure in the accelerated growth regime followed by accentuated closure in the retardation regime. By contrast, measurement of the mid-thickness elastic strain field behind and ahead of the crack made by synchrotron X-ray diffraction showed no evidence of significant crack-face contact stresses immediately behind the crack-tip on approaching minimum loading. Though the results were affected by point-to-point scatter due to an insufficiently small grain size, the changes during loading and overloading could mostly be explained by a simple elastic plastic analysis using a value of the yield stress intermediate between the initial yield stress and the ultimate tensile stress (UTS). This showed very significant compressive plastic strains ahead of the crack that start to form early during unloading.

Here we revisit this topic by studying a bainitic rather than stainless steel. This has an inherently much finer grain size allowing us to achieve much higher spatial resolution in the X-ray diffraction data with much reduced point to point scatter [22]. Further the steel has sufficient toughness that a large plastic zone can be introduced in contrast to the Al-Li studied by Steuwer et al. [23]. This has enabled us to study the elastic strain field and the effect of plasticity on closure in unparalleled detail.

2. MATERIAL AND SPECIMEN

A compact tension (CT) fatigue specimen was machined from quenched and tempered bainitic steel similar to Q1N (HY80) [24]. Its chemical composition is summarised in Table 1. The tensile properties are as follows: Yield Stress (σ_y) = 690 MPa and Ultimate Tensile Stress, σ_{uts}= 858 MPa. The CT specimen had a width of 60 mm [25] and thickness of 3.3mm.

3. EXPERIMENTAL SETUP

The crack-tip elastic strain fields were measured on the energy dispersive ID15 beamline at the European Synchrotron Radiation Facility (ESRF), using the same arrangement as that described in [23] and shown schematically in Fig. 1a. The scattering angle was $2\theta = 5^{o}$. The incident beam slits were opened to $60 \times 60\ \mu m^2$ giving a lateral resolution (x,y) of 60μm and a nominal gauge length through-thickness (z) of around 1.4 mm (diamond shaped centred on the mid-plane (z=0)) [26]. This allowed a 10 times greater spatial resolution than in previous elastic strain field mapping experiments for plastically extended crack-tips [21]. Such a good resolution was possible because of the small grain size of the bainitic steel used here.

The DIC was undertaken simultaneously using a single camera set-up shown in Fig. 1 [15] taking contrast from the speckle pattern arising from paint applied to the region to be monitored. The slightly oblique view of the sample was corrected for before the analysis of the data. Commercial DIC analysis software (La Vision GmbH, Gottingen, Germany) [27] was used to analyse the results and details of the approach are provided in [28]. For all images the correlation was done by using the state at K_{min} prior to OL as the reference image.

In this experiment the loading rig was accommodated upon the sample table of ID15. Great care was taken to correct for slight sample movements that took place when the sample was fatigued and when it was statically loaded to K_{max} (=35MPa√m) and K_{min} (=1.2MPa√m) to ensure that all of the strain maps were recorded with respect to the sample coordinates and not the lab coordinates. To this end both shifts recorded by DIC analysis and by edge scans by synchrotron XRD were used. It is estimated that we were able to correct the in-plane sample location to ±50μm.

4. FATIGUE EXPERIMENT

The specimen was fatigue pre-cracked for 3000 cycles at a frequency of 10Hz at a stress intensity range, ΔK, of approximately 35MPa√m and load ratio, K_{min}/K_{max}, of 0.03. Since each XRD measurement included information averaged over 1.4 mm through the thickness, plane stress conditions dominated through the thickness for all loads applied during the experiment [29]. The crack length was measured perpendicularly to the loading direction from the centre of the loading holes [25]. Once the fatigue crack had grown to a length of 12.75 mm, a 67% overload (OL) was applied (i.e. one cycle having a maximum load 1.67 times the maximum

load in the baseline cycles). Strain measurements were made over a number of fatigue stages, namely during the last cycle just before the overload (OL-1), during the overload (OL), 40 cycles after the overload (OL+40), 2040 cycles after the overload (OL+2k), 8040 cycles after the overload (OL+8k) and 37540 cycles after the overload (OL+37k). In addition to 2D maps, a profile of the evolution of strain behind and ahead of the crack-tip was produced for each of the fatigue stages studied by measuring around 50 strain points along the crack plane (y=0) at different distances from the location of the crack at overload. The crack growth in the specimen was measured using XRD line scans and is summarised in Table 2. These values were used for correcting the location of the crack-tip at each loading stage in the subsequent sections.

5. SURFACE AND BULK MEASUREMENTS

The elastic strains were measured directly from the diffraction profiles to obtain the lattice spacing representative of the (211) diffraction peak. High quality elastic strain maps were obtained showing very little point-to-point scatter which are shown with no smoothing or filtering. The elastic strains parallel to the loading direction (ε_{yy}) and parallel to the crack growth direction (ε_{xx}) are shown in Fig. 2 at the overload. The elastic strain fields are broadly similar in shape and magnitude to those recorded by Steuwer et al. [23]. The images taken from the surface of the sample were analysed using LaVision Davis v8.0 employing a least square algorithm with subset size 31 (patch size) and step size 8 pixels (75% overlap).
The corresponding total (elastic plus plastic) strains recorded at OL were obtained from DIC and are also shown in Fig 2. Unsurprisingly, the elastic strains are 5-10 times smaller than the total strains local to the crack due to plastic deformation. A simple Irwin analysis predicts a plastic zone of around 2.5mm for the overload event (61MPa√m). The DIC shows clearly the characteristic plastic lobes.

Unfortunately it is not possible to measure the through-thickness elastic strain ε_{zz} using the synchrotron beam with the same spatial definition as the two in-plane strains [26], however the stresses can be inferred using the relations for plane stress ($\sigma_{zz} = 0$):

$$\sigma_{yy} = \frac{E}{1-\nu^2}\left[\varepsilon_{yy} + \nu\varepsilon_{xx}\right] \quad (1)$$

The stress in the vicinity of the crack-tip in the loading direction for the OL cycle at maximum and minimum loads are shown in Figures 3a and 3b, respectively. Fig. 3a clearly shows the classical butterfly stress field (HRR field) formed around the crack-tip. Note the different

colours scales used in Fig. 3a and 3b and the fact that the yield stress is 690MPa. The 2D elastic stress field within the plastic zone has not been mapped in previous studies. The DIC data allow the crack opening displacement to be mapped in the vicinity of the crack (Fig. 4a). This was carried out by fitting a series of heaviside functions to the vertical profiles of the vertical displacements to identify the discontinuity in the displacement caused by the faces of the crack opening. Fig. 4b shows the evolution of ΔCOD for all fatigue stages. It is observed that the crack opening increases with distance to crack-tip, as it is expected. The OL cycle shows the highest ΔCOD, followed by OL-1 and OL+37k. ΔCOD shows very little change between fatigue stages OL+40 and OL+8k. DIC data in Fig. 2 suggests that the plastic zone extends 2-3mm ahead of the crack-tip although its magnitude falls away quickly. This can be seen in the butterfly-like shape that is observed in Fig. 2c extending from x= -0.5 and to x=+1.5 mm. The residual stress field shows a slight tensile hump around 2.5mm ahead of the crack (see later discussion).

Fig. 5c shows the difference between maximum and minimum stress. Fig. 5a shows a strong gradient of stress at the crack-tip, followed by a smooth decrease ahead of the crack-tip. The maximum stress is achieved in the OL, followed by OL+37k and OL-1. OL+40 to OL+8k show smaller stress values than other fatigue stages up to ~1.5 mm ahead of the crack. Fig. 5b shows that for the minimum load, all fatigue stages except OL-1 and OL+37k have a large trough at the crack-tip with compressive stress of ~1000 MPa. Fig. 5c shows that stress difference between maximum and minimum load is maximum for the OL case. Fig. 5c shows a very similar stress evolution in all fatigue stages but the OL stage. Similar profiles were previously measured on Al-Li alloy [11]. Even though the spatial resolution was greater in the previous work [11] (40 μm in the previous work and 60μm in the current work), the larger plastic zone in the current steel allowed the crack-tip field to be resolved with better accuracy. Around 40 strain data points were measured over the current OL plastic zone, whereas only 12 strain data points were measured previously through the OL plastic zone.

6. POST-PROCESSING OF STRAIN DATA

The COD profiles shown in Fig. 4b clearly show differences in opening displacement. Since the nominally applied ΔK was constant, the COD differences are likely due to changes in the opening load. Due to beam time restrictions, it was not possible to monitor by XRD and DIC the loading or unloading part of the cycle for each fatigue stage, but only at maximum and

minimum load for each fatigue stage. Consequently, the opening load can not be quantified directly. Nevertheless, the evolution of the COD along the wake can be used to estimate the opening load as follows. COD information is available from ~5 mm behind the crack tip to ~3 mm ahead of the crack-tip. Displacement values 5 mm behind the crack-tip were considered for estimating the opening load, since they present better signal to noise ratio (see Fig. 4b) and because it is recommended to use data as remote as possible from the crack-tip [30]. The COD for all fatigue stages at maximum load is summarised in Table 3.

The opening load for the OL-1 stage can be estimated as [31]:

$$\frac{P_{op}}{P_{\max}} = A_0 + A_1 R + A_2 R^2 + A_3 R^3 \quad (2)$$

where P_{op} is the opening load, P_{max} is the maximum nominally applied load, R is the load ratio, A_0, A_1, A_2 and A_3 are coefficients dependent on applied stress, yield stress and the stress/strain state. Plane stress conditions were assumed. The maximum nominally applied load, P_{max}, is 5.3 kN and the load ratio, R is 0.03. The opening load for OL-1 was estimated with equation (2) to be 2.3 kN. The opening load for fatigue stages OL+40, OL+2k, OL+8k and OL+37k was estimated from compliance curves. Compliance curves were drawn combining the COD profiles (Fig. 4b) with the opening load for OL-1.

The compliance curve for OL-1 was generated as follows. Below the opening load, the crack was assumed to remain closed and so the COD was 0 for loads up to 2.3 kN. At maximum load, the COD for OL-1 is that shown in Table 3. The crack was assumed to open gradually from 0 μm at the opening load (2.3 kN) up to 28.6 μm at maximum load. The compliance curves for other fatigue stages were drawn assuming the same slope as OL-1 and taking into account the change in COD at maximum load (see Table 3). The compliance curves are shown in Fig. 6a and can be used to estimate the opening load for other fatigue stages from the crossing point with the load axis. The opening load against the crack growth are plotted in Fig. 6b for all fatigue stages except for the OL cycle.

7. DISCUSSION

The effect of the compressive residual stress field, which has been generated at the crack-tip by the overload, on the peak stress in the loading direction after (OL+40) compared with that measured before the (OL-1) overload is evident in Fig. 5a. A 42% decrease is observed in the

maximum stress in the crack loading direction near the crack-tip before and after applying a 67% overload. 38% decrease was observed previously in thick specimen made of the same steel with a 100% overload [22]. This means that the decrease induced by the overload is proportionally larger in the thin sample than in the thick sample. The magnitude of the residual stress induced by the overload can be estimated by comparing the peak compressive stress just ahead of the crack-tip before and after the overload (see Fig. 5b). As can be seen in the figure the maximum compressive stress at K_{min} just before the overload is approximately -550 MPa which rises to almost -1000 MPa immediately after the overload.

It is clear from Fig. 5c that the elastic change in stress in the crack-tip region upon loading to K_{max} is essentially the same as that for the baseline fatigue cycle (OL-1) for all the post overload cycles, it is just that post OL the cycles are offset by the compressive residual stress field introduced by the OL event. This is consistent with the observations of Lopez-Crespo et al. [22] for a thick (plane strain) CT sample of the same steel.

The change in crack opening displacement (ΔCOD) between minimum and maximum load with distance behind the crack-tip is shown in Fig. 4b. Unsurprisingly the crack opening is much greater at OL than prior to it (OL-1). After OL the crack opening displacement appears to be reduced (by around 30%) at K_{max} relative to OL-1 for the first 8k cycles returning to a level similar to that for OL-1 after 37k cycles. The reduction in the change in crack opening (i.e. crack opening displacement between first K_{min} before OL and K_{max} at each loading state) displacement can be interpreted as 54% reduction in the effective stress intensity factor range and is consistent with plasticity-induced crack closure. Given the resolution of the DIC system, the crack can be assumed to be closed if COD < 2.5μm. Accordingly, the crack length can be fictitiously reduced by 1mm for OL-1 and OL+37k and by 2mm for OL+40, OL+2k and OL+8k. This may be because closure effects which might be expected to be most prominent on the surface where the DIC measurements are made, does not allow the crack to open beyond the resolution of the DIC and therefore gives the impression of a shorter crack. While DIC seems to capture the transient behaviour at the surface after the OL event with different ΔCOD curves at OL+8k and OL+37k (Fig. 4b), XRD does not show noticeable differences after the OL (Fig. 5c).

There are a number of other interesting features relating to the stress profiles shown in Fig. 5. Most importantly, it is evident that only when the crack has grown through the compressive residual stress field introduced with the OL, does the COD or the peak crack-tip elastic strain field revert to that representative of the original baseline fatigue response (OL-1). Secondly,

the ‘hump’ in the stress in the crack-opening direction which arises 2.5mm ahead of the crack when the overload is applied and retained for the OL+40, +2k and +8k cycles but is not present for the baseline fatigue or for the last increment. Because the unload curves are elastic the ‘hump’ is also evident in the unloaded profiles too. Both these observations are almost certainly connected to the fact that only after 37k cycles has the crack-tip grown sufficiently (by 2.05mm) to have emerged from the plastic zone introduced by the overload. Such ‘hump’ could not be observed in a similar experiment conducted on a thicker specimen [22] which suggests that it is specific to thin CT specimens. We are currently conducting ultrafine FEM [32] to understand the origin of such ‘hump’.

The compliance curves in Fig. 6a were estimated assuming equal stiffness of the CT specimen for the different fatigue stages. They are an approximation since the specimen actually becomes more compliant as the crack grows (i.e. the slope in Fig. 6a should increase slightly as the crack grows). Such correction would imply opening loads higher than those estimated from Fig. 6a for stages after the OL. In addition, curves in Fig. 6a show a simplified pure linear elastic behaviour. Real compliance curves would also be affected by plasticity, thus affecting the opening load. The small increase in COD that occurs for loads below the opening load was assumed to be zero. The estimated values of opening load are useful to illustrate the influence of the OL event. Fig. 6b suggests that a single 67% OL cycle raises the opening load by 30% soon after the OL was applied (OL+40). Very little change in the opening load was observed for the following 8000 cycles. Finally, it is observed that the for OL+37k condition, the opening load goes back to approximately the values prior to the OL. The ratio opening load to maximum load was 43% in the OL-1 fatigue stage and 57% in the OL+40 fatigue stage. Similar P_{op}/P_{max} values were observed on a 316L steel subjected to 100% OL [15]. Nevertheless, interesting differences are observed between the two studies. While in the current work the maximum P_{op}/P_{max} values were achieved soon after the OL event took place, previously [15] the maximum P_{op}/P_{max} value was achieved at a much later stage. This difference suggests that the extension of the OL might relate to the extent of the OL as compared to the baseline cycles.

Fig. 6b indicates that the extension of the OL retardation is at most 2.05 mm, which agrees well with the size of the monotonic plastic zone estimated by Irwin approximation (2.1 mm). Given the limited time available to conduct the synchrotron experiment, it was not possible to assess the opening load at various other stages between OL+8k and OL+37k. The data

available in this study suggests that the influence of the OL is between the minimum and maximum zones of OL influence shown in Fig 6b.

8. CONCLUSIONS

X-ray diffraction and digital image correlation techniques were simultaneously applied to measure the change in the elastic and plastic strain fields around a fatigue crack after an overload. The DIC surface strain measurements are consistent with a plastic zone extending some 2-3mm ahead of the crack-tip; while the stresses recorded by diffraction show a slight tensile hump 2.5mm ahead of the crack-tip. Both the elastic strain field measured by XRD and the crack opening displacement measured by DIC showed a reduction in their peak values as a result of the compressive residual stress field induced around the crack-tip after the overload. Once the crack had grown through the plastic zone, both the change in crack opening displacement and the peak tensile crack-tip stress field returned to levels similar to that prior to the overload condition. The crack-tip stress field changes over each cycle were broadly the same before and at all stages after OL.

ACKNOWLEDGEMENTS

The authors are grateful to the ESRF for ID15 beam-time awarded under MA1483. Financial support of Junta de Andalucía through Proyectos de Excelencia grant reference TEP-3244 is greatly acknowledged. Funding under EPSRC grant EP/M010619/1 is also acknowledged.

REFERENCES

[1] Srawley JE. On the sharpness of crack compared with Wells' COD. NASA TMS-529040; 1970.
[2] Suresh S. Micromechanisms of fatigue crack growth retardation following overloads. Engineering Fracture Mechanics. 1983;18:577-593.
[3] Jones RE. Fatigue crack growth retardation after single-cycle peak overload in Ti–6Al–4V titanium alloy. Engineering Fracture Mechanics. 1973;5:589-604.
[4] Elber W. Fatigue crack closure under cyclic tension. Engineering Fracture Mechanics. 1970;2:37-45.
[5] Vasco-Olmo JM, Díaz FA, Patterson EA. Experimental evaluation of shielding effect on growing fatigue cracks under overloads using ESPI. International Journal of Fatigue, accepted http://dxdoiorg/101016/jijfatigue201510003. 2015.

[6] Hutchings MT, Hippsley CA, Rainey V. Neutron Diffraction Measurement of the Stress Field During Fatigue Cycling of a Cracked Test Specimen. Mat Res Soc Symp Proc. 1990;166:317.
[7] Lee SY, Liaw PK, Choo H, Rogge RB. A study on fatigue crack growth behavior subjected to a single tensile overload Part I. An overload-induced transient crack growth micromechanism. Acta Materialia. 2011;59(2):485-494.
[8] Steuwer A, Santisteban JR, Turski M, Withers PJ, Buslaps T. High-resolution strain mapping in bulk samples using full-profile analysis of energy dispersive synchrotron X-ray diffraction data. Nucl Instr Meth Physics Research B. 2005;238B:200-204.
[9] Croft M, Zhong Z, Jisrawi N, Zakharchenko I, Holtz RL, Skaritka J, Fast T, Sadananda K, Lakshmipathy M, Tsakalakos T. Strain profiling of fatigue crack overload effects using energy dispersive X-ray diffraction. International Journal of Fatigue. 2005;27(10-12):1408-1419.
[10] Withers PJ. Fracture mechanics by three-dimensional crack-tip synchrotron X-ray microscopy. Philosophical Transactions of the Royal Society A-Mathematical Physical and Engineering Sciences. 2015;373:20130157.
[11] Steuwer A, Rahman M, Shterenlikht A, Fitzpatrick ME, Edwards L, Withers PJ. The evolution of crack-tip stresses during a fatigue overload event. Acta Materialia. 2010;58:4039-4052.
[12] Mokhtarishirazabad M, Lopez-Crespo P, Moreno B, Lopez-Moreno A, Zanganeh M. Evaluation of crack-tip fields from DIC data: a parametric study. International Journal of Fatigue. 2016; published online, DOI 10.1016/j.ijfatigue.2016.03.006.
[13] Sutton MA, McNeill SR, Helm JD, Boone ML. Measurement of crack tip opening displacement and full-field deformations during fracture of aerospace materials using 2D and 3D image correlation methods. Iutam Symposium on Advanced Optical Methods and Applications in Solid Mechanics. 2000;82:571-580.
[14] Nowell D, de Matos PFP. Application of digital image correlation to the investigation of crack closure following overloads. In: Lukas P, editor. Fatigue 2010, 2010. p. 1035-1043.
[15] Yusof F, Lopez-Crespo P, Withers PJ. Effect of overload on crack closure in thick and thin specimens via digital image correlation. International Journal of Fatigue. 2013;56:17-24.
[16] Lopez-Crespo P, Shterenlikht A, Yates JR, Patterson EA, Withers PJ. Some experimental observations on crack closure and crack-tip plasticity. Fatigue and Fracture of Engineering Materials and Structures. 2009;32:418-429.
[17] Mostafavi M, Schmidt M, Marsden BJ, T.J. Marrow. Fracture behaviour of an anisotropic polygranular graphite (PGA) Materials Science and Engineering: A. 2012;558:265-277.
[18] Lopez-Crespo P, Shterenlikht A, Patterson EA, Withers PJ, Yates JR. The stress intensity of mixed mode cracks determined by digital image correlation. Journal of Strain Analysis for Engineering Design. 2008;43:769-780.
[19] Lopez-Crespo P, Burguete RL, Patterson EA, Shterenlikht A, Withers PJ, Yates JR. Study of a crack at a fastener hole by digital image correlation. Experimental Mechanics. 2009;49:551-559.
[20] Becker TH, Mostafavi M, Tait RB, Marrow TJ. An approach to calculate the J-integral by Digital Image Correlation displacement field measurement Fatigue and Fracture of Engineering Materials and Structures. 2012;35:971-984.
[21] Lopez-Crespo P, Withers PJ, Yusof F, Dai H, Steuwer A, Kelleher JF, Buslaps T. Overload effects on fatigue crack-tip fields under plane stress conditions: surface and bulk analysis. Fatigue and Fracture of Engineering Materials and Structures. 2013;36(1):75-84.

[22] Lopez-Crespo P, Steuwer A, Buslaps T, Tai YH, Lopez-Moreno A, Yates JR, Withers PJ. Measuring overload effects during fatigue crack growth in bainitic steel by synchrotron X-ray diffraction. International Journal of Fatigue. 2015;71:11-16.
[23] Steuwer A, Rahman M, Shterenlikht A, Fitzpatrick ME, Edwards L, Withers PJ. The evolution of crack-tip stresses during a fatigue overload event. Acta Mater. 2010;58(11):4039-4052.
[24] Robertson IM. Measurement of the effects of stress ratio and changes of stress ratio on fatigue crack growth rate in a quenched and tempered steel. . Int J Fatigue. 1994;16:216-220.
[25] Murakami Y. Stress Intensity Factors Handbook. Oxford: Pergamon Press, 1987.
[26] Withers PJ. Synchrotron X-ray Diffraction. In: Schajer GS, editor. Practical residual stress measurement methods: John Wiley, 2013. p. 163-176.
[27] LaVision, Digital Volume Correlation - DAVIS 8.0 Product Manual , Gottingen, 2010.
[28] Quinta da Fonseca J, Mummery PM, Withers PJ. Full-field strain mapping by optical correlation of micrographs acquired during deformation. J Micros. 2005;218:9-21.
[29] Anderson TL. Fracture Mechanics, Fundamentals and Applications. CRC Press, 2005.
[30] ASTM E647 Standard test method for measurement of fatigue crack growth rates. 2005.
[31] Newman JC. A crack opening stress equation for fatigue crack growth. International Journal of Fracture. 1984;24:R131-R135.
[32] Garcia-Manrique J, Camas D, Lopez-Crespo P, Gonzalez-Herrera A. Stress intensity factor analysis of through thickness effects. International Journal of Fatigue. 2013;46:58-66.

Tables

Alloy	C	Si	Mn	P	S	Cr	Ni	Mo	Cu
Q1N	0.16	0.25	0.31	0.010	0.008	1.42	2.71	0.41	0.10

Table 1: Chemical composition in weight % of Q1N steel. The balance is Fe.

Fatigue stage	OL+40	OL+2K	OL+8K	OL+37K
Crack growth	0.08	0.22	0.27	2.05

Table 2: Crack growth in mm relative to the crack length at OL.

Fatigue stage	OL-1	OL+40	OL+2K	OL+8K	OL+37K
COD at maximum load	28.6	21.9	22.7	22.8	29.2

Table 3: COD vales in μm measured 5 mm behind the crack-tip.

Figures

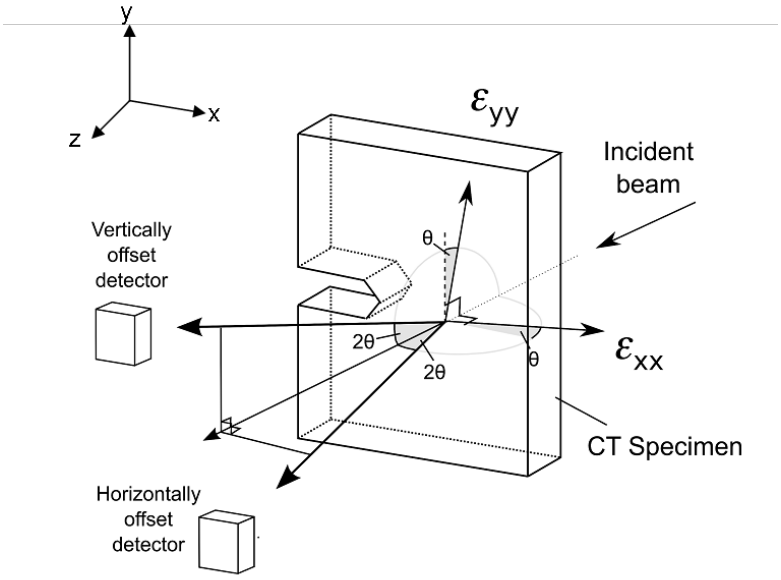

(a)

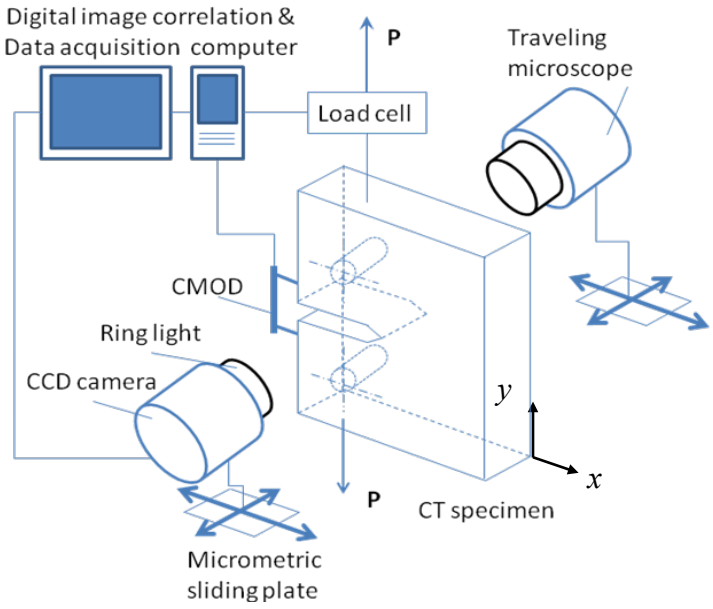

(b)

Figure 1: Schematics showing a) the energy dispersion diffraction geometry with two detectors so as to measure two in-plane directions of strain; note the coordinate system for ε_{xx} and ε_{yy}. For very low θ, these strains can be taken as representative of those in the loading (y) and crack growth (x) directions, b) the DIC arrangement [15]. In actual fact the camera viewed the sample at a slight angle to allow the X-ray beam unimpeded access to the sample.

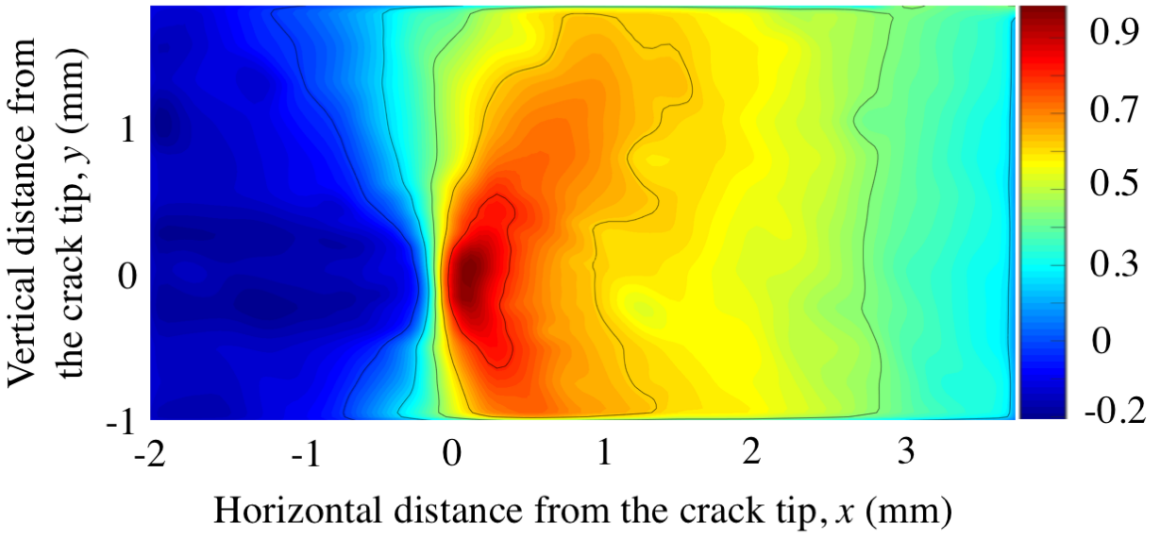
Vertical distance from the crack tip, y (mm)
1
0
-1
-2
-1
0
1
2
3
Horizontal distance from the crack tip, x (mm)
0.9
0.7
0.5
0.3
0
-0.2

(a)

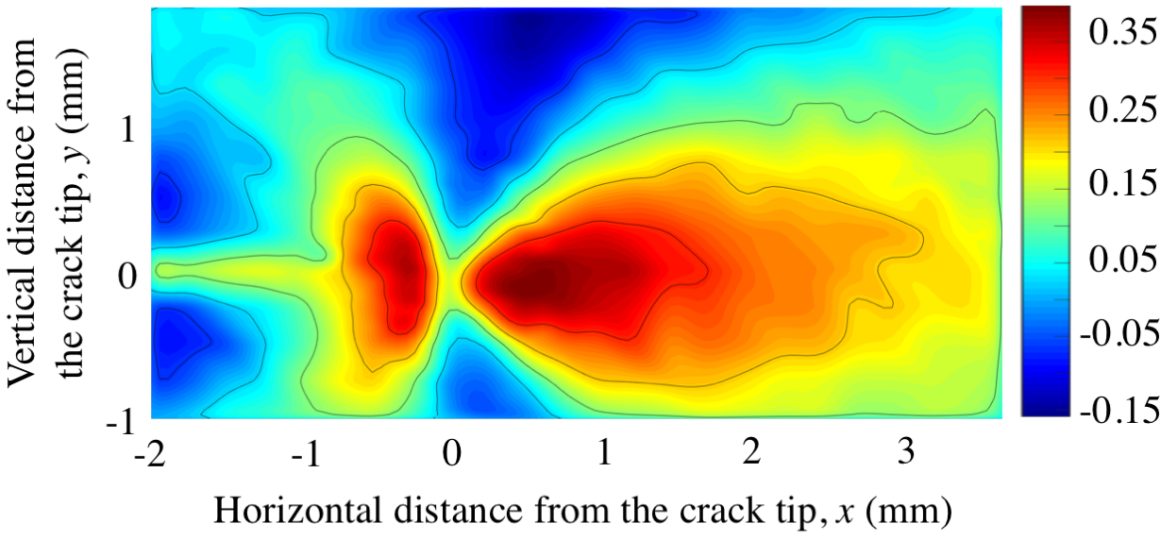
Vertical distance from the crack tip, y (mm)
1
0
-1
-2
-1
0
1
2
3
Horizontal distance from the crack tip, x (mm)
0.35
0.25
0.15
0.05
-0.05
-0.15

(b)

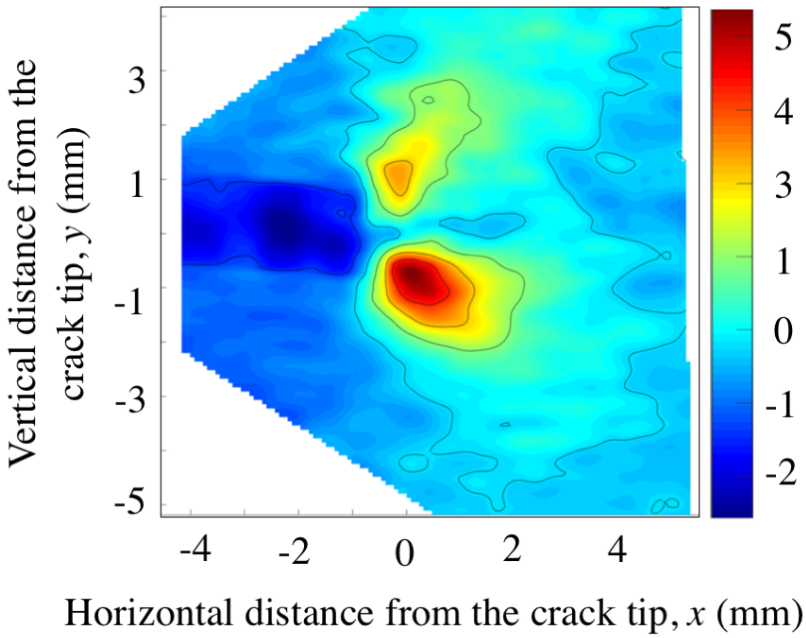

(c)

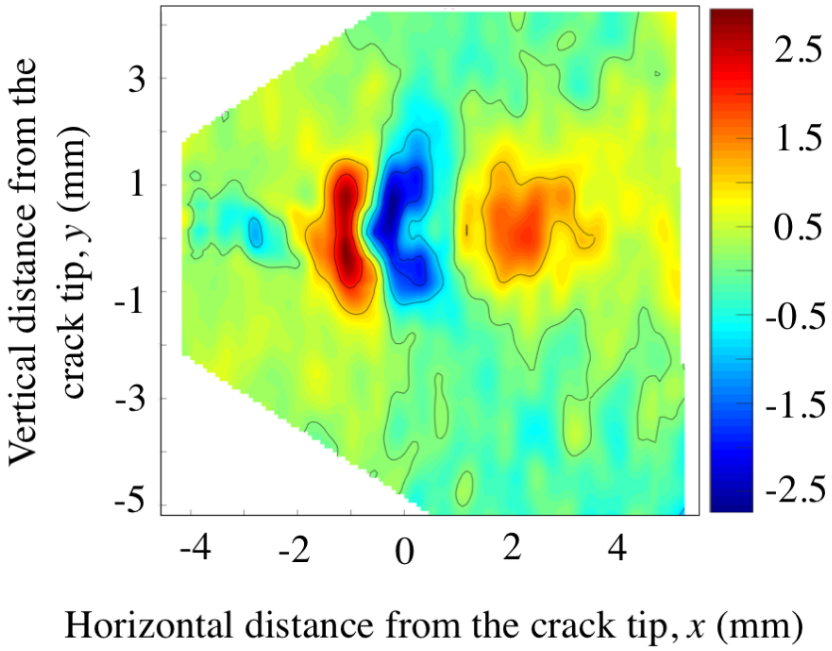

(d)

Figure 2: Strain maps (in %) at overload (OL) showing the elastic strains measured by XRD in the a) loading direction ε_{yy} and b) parallel to the crack growth direction ε_{xx} and the total strain measured by DIC in the c) loading direction ε_{yy}^{tot} and d) parallel the crack growth direction ε_{xx}^{tot}. The XRD measurements were performed while the sample was loaded at the maximum load ($1.7K_{max}$); the DIC strains were calculated from full-field displacements measured by comparing the images of the surface of the sample taken at maximum load ($1.7K_{max}$) and minimum load (K_{min}) for the cycle just before the overload.

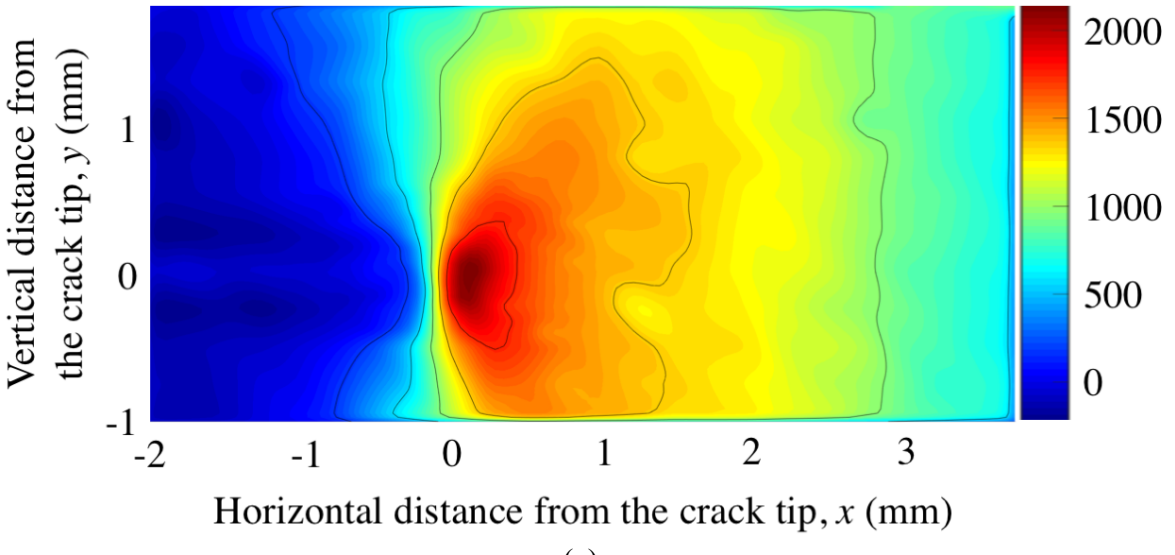

(a)

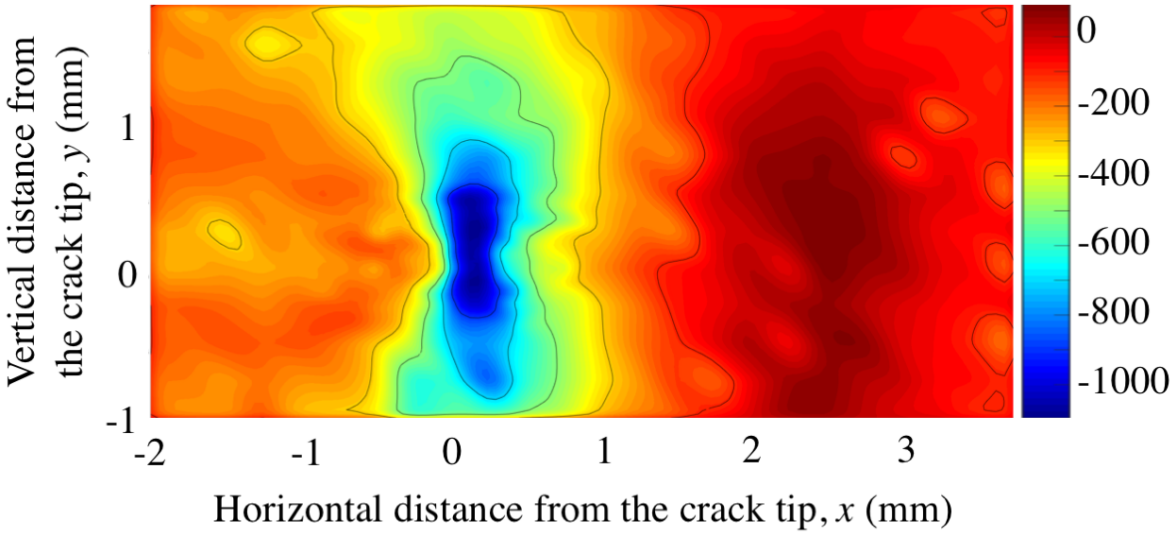

(b)

Figure 3: Mid-plane maps of stress in the loading direction σ_{yy} (in MPa) calculated from the elastic ε_{xx} and ε_{yy} measured by synchrotron XRD a) at OL ($1.7K_{max}$) and b) immediately after OL at minimum load (K_{min}).

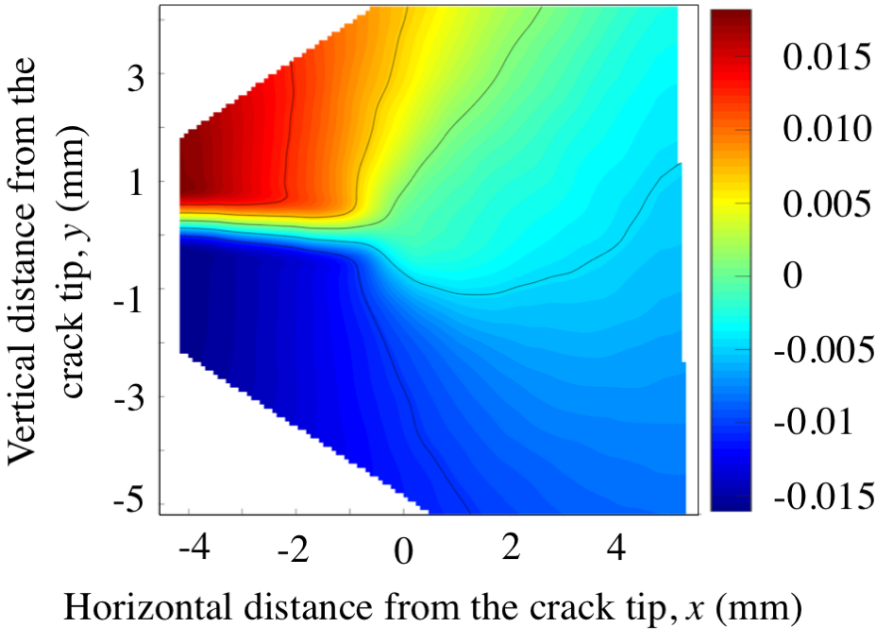

(a)

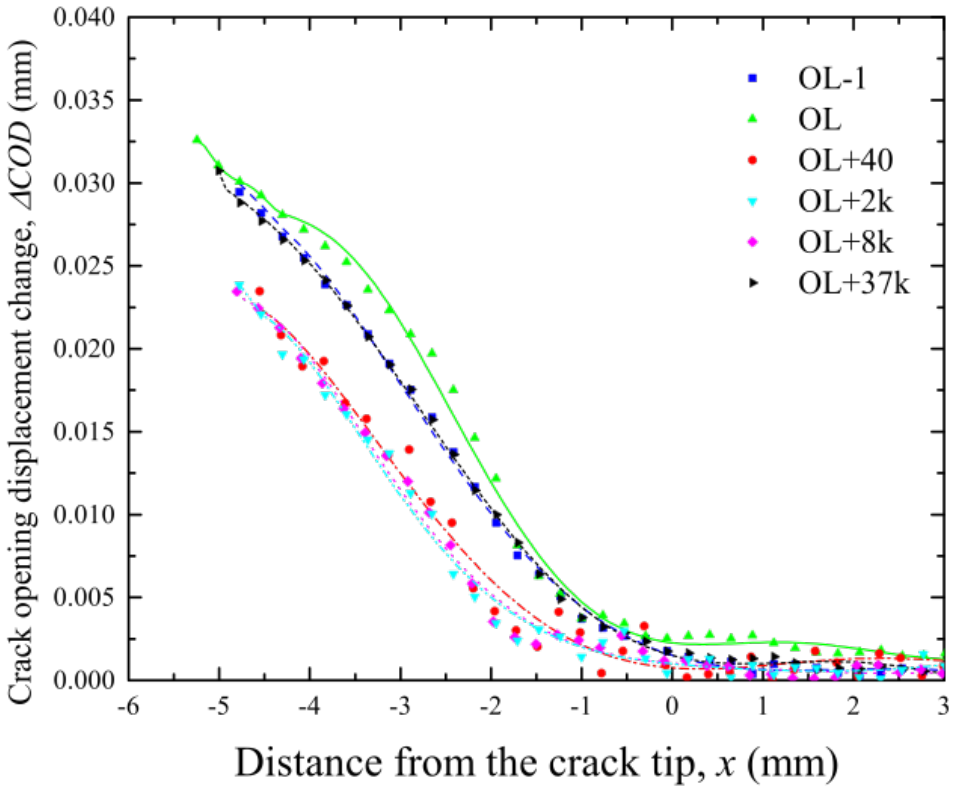

(b)

Figure 4: DIC analysis showing the a) vertical displacement field V_y (in mm) between $1.7K_{max}$ (OL) and K_{min} just prior to OL, b) change in crack opening displacement (ΔCOD) profiles for each fatigue stage.

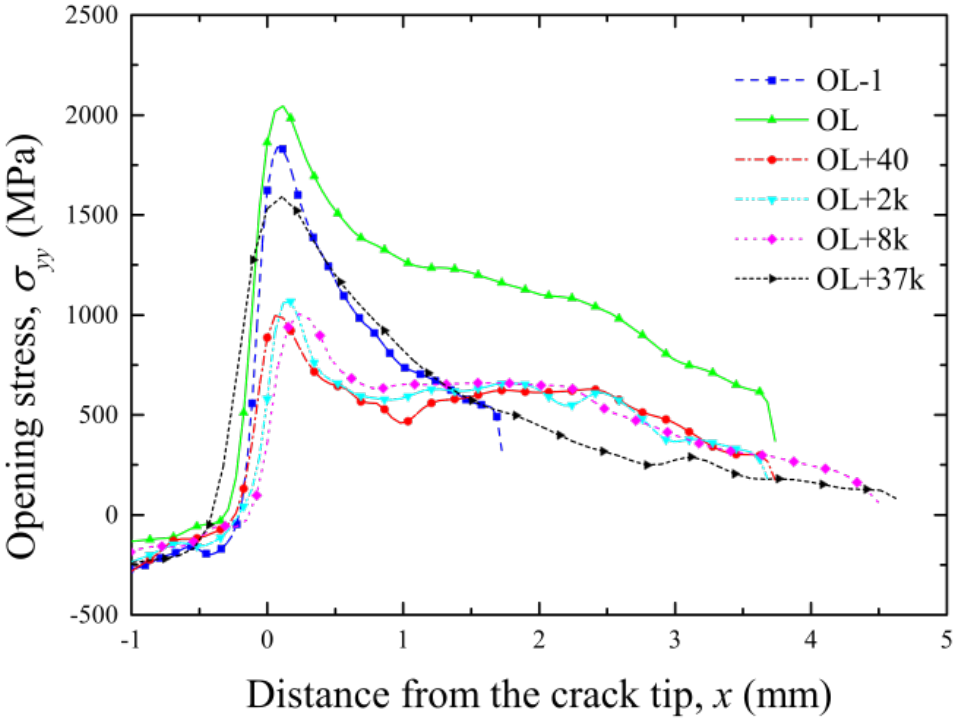
OL-1
OL
OL+40
OL+2k
OL+8k
OL+37k
Opening stress, σ_{yy} (MPa)
Distance from the crack tip, x (mm)
2500
2000
1500
1000
500
0
-500
-1
0
1
2
3
4
5

(a)

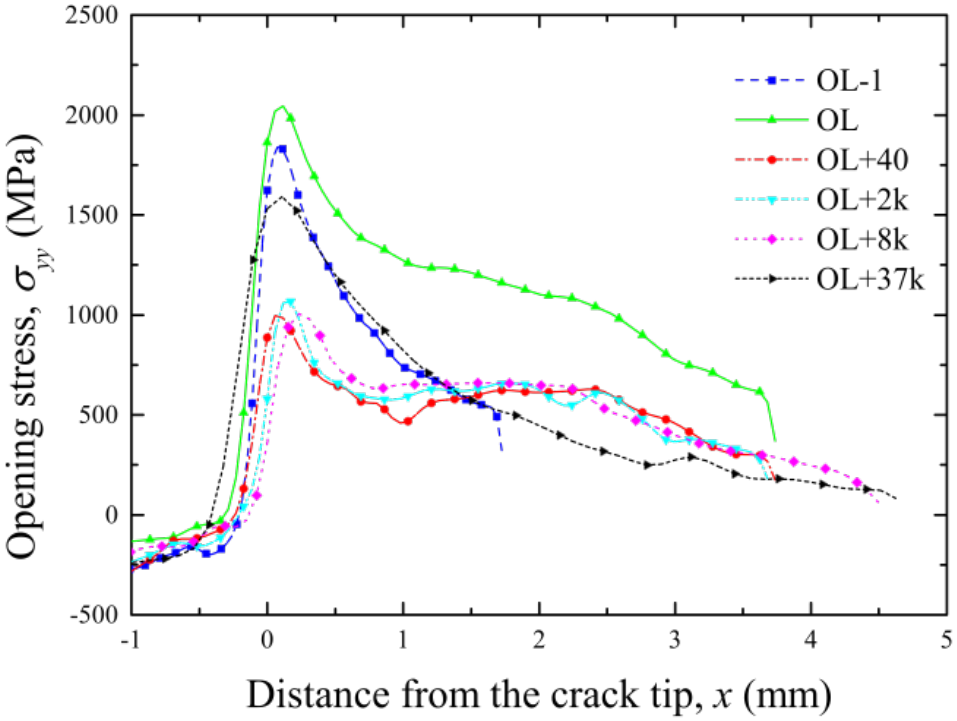
OL-1
OL
OL+40
OL+2k
OL+8k
OL+37k
Opening stress, σ_{yy} (MPa)
Distance from the crack tip, x (mm)
2500
2000
1500
1000
500
0
-500
-1
0
1
2
3
4
5

(b)

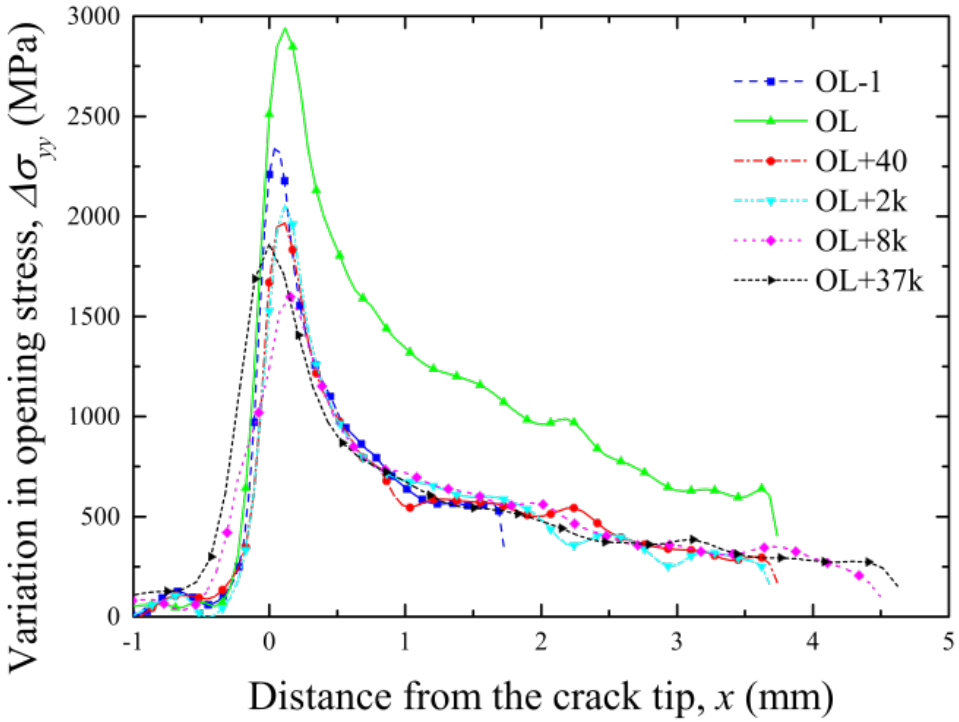

(c)

Figure 5: Synchrotron XRD line profiles along y=0 showing the crack loading stress σ_{yy} a) at maximum load, b) at minimum load and c) the difference between the stresses at maximum and minimum load at each stage in the fatigue crack growth response.

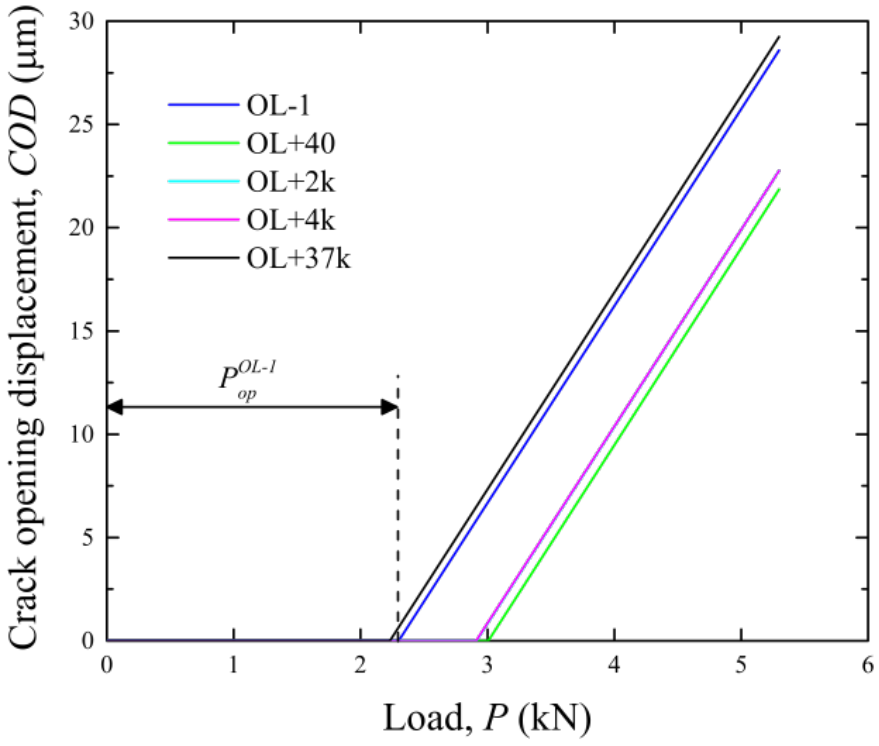

(a)

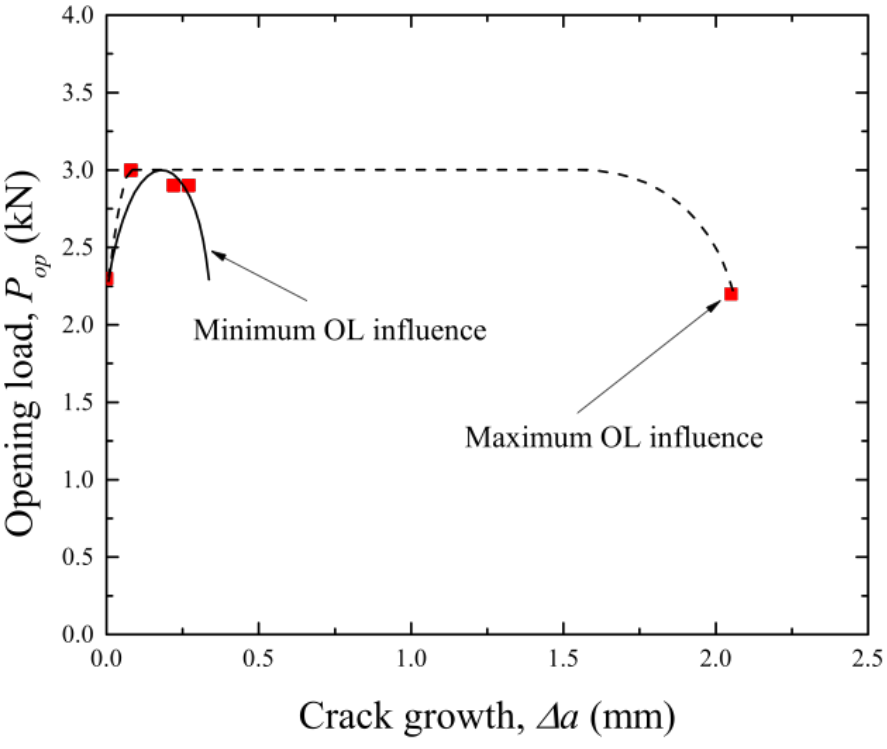

(b)

Figure 6. a) Estimated compliance curves and b) evolution of opening load with crack growth for different crack lengths. Crack growth in b) is measured from the crack length at the OL condition. The minimum and maximum zone of influence of the OL are shown with solid and dashed lines respectively. The maximum load for the baseline cycles is 5.3 kN.